

A PML for Electroacoustic Waves in Piezoelectric Materials Using FDTD

Arthur O. Montazeri, Mohamed H. Bakr, and Yaser M. Haddara

Department of Electrical and Computer Engineering
 McMaster University, Hamilton, ON, L8S 1M6, Canada
 montazo@mcmaster.ca, mbakr@mail.ece.mcmaster.ca, yaser@mcmaster.ca

Abstract — A perfectly matched layer (PML) is introduced for elastodynamic waves in piezoelectric materials. A matching condition is derived for the PML equations to reduce spurious reflections from the boundary. The finite difference time domain (FDTD) is used to model the propagation of the wave in the piezoelectric material. The results show good performance of the proposed PML boundary.

Index Terms — Elastodynamic wave, FDTD, piezoelectric materials, PML, SAW.

I. INTRODUCTION

Much interest is devoted to the surface acoustic wave (SAW) devices due to the versatility of their application and their widespread use. SAW-based resonators and delays are readily used in commercial telecommunication systems [1]. This makes any error reduction method, before the onset of fabrication, an extremely powerful tool for the industry. It also highlights the use of the computer aided design software in determining the SAW device responses prior to manufacturing.

Surface acoustic wave simulators are generally categorized into two groups: behavioural models and physics-based models [2,3]. Behavioural models, also known as phenomenological models, are employed to quickly obtain the device response, typically by expanding the response in terms of certain basis functions [4]. On the other hand, physics-based models, also referred to as full-wave models, are more accurate. They directly solve the differential equations of SAW generation [3]. There is also another fundamental difference

between the two: physics-based models need only be supplied with the boundary conditions of the problem, the excitation, and the initial conditions. Behavioural techniques, on the other hand, require a set of parameters describing an already-existing wave. These parameters are either extracted from experimental measurements, or from physics-based simulations. A popular behavioural modeling approach is the coupling-of-modes (COM) method explained in [3]. References describing other phenomenological models exist [3, 5-7]. As a result, the two simulation methodologies are often complementary, rather than competitive.

Frequency domain techniques are in particular powerful for determining SAW device responses at specific frequencies [6]. On the other hand, in order to obtain a wideband device response, a large number of such simulations are required. This is where time domain techniques prove their worth [8]. Most SAW device modeling has been done in the frequency domain, and so a wider selection of boundary conditions including the PML is available in the frequency domain.

At the same time, time domain techniques such as FDTD, provide a powerful tool for wideband frequency response simulation. FDTD can also incorporate anisotropic media which include all piezoelectric materials. These properties make FDTD a suitable candidate for simulating micro-acoustic devices [9].

In this paper, we develop an FDTD physics-based model through the discretization of the piezoelectric governing equations. We describe an improvement to reduce spurious reflections from the PML boundary. PML implementations for this

type of structure based on existing recipes cause instabilities for certain crystal groups [9]. Here, a PML for acoustic waves is derived by closely following Bérenger's derivation of a PML for electromagnetic waves. A new matching condition is developed to relate the velocity and stress loss-coefficients similar to the matching condition defined for electromagnetic waves.

Our paper is organized as follows: In Section II, SAW devices are introduced along with an overview of absorbing boundary conditions. In Section III, our parallel derivation of a PML for the elastodynamic wave equation is given. We present the PML time update equations based on the derived matching condition. Finally, Section IV presents the results.

II. BACKGROUND

A. SAW generation and propagation

In the SAW devices considered here, surface acoustic waves are generated by the application of an excitation to a thin metal interdigital transducer (IDT) deposited on the free surface of a piezoelectric substrate, as shown in Fig. 1.

Generally, two IDTs, separated on the surface of the piezoelectric substrate, constitute a basic two-port SAW device. One IDT acts as a transmitter and the other as a receiver. The transmitting IDT converts the electrical signal into mechanical wave vibrations, which travel through the medium to reach the receiver IDT. Through the piezoelectric effect, the mechanical SAW wave is converted back into an electrical output signal. The two-port devices considered here are compliant with the reciprocity theorem, where switching the transmitter and receiver ports will have no effect on the device functionality [1].

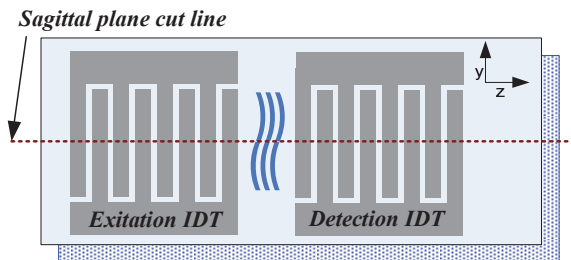


Fig. 1. A 2-port SAW device.

In the IDT region of the wave generation zone, the substrate should be piezoelectric. The region in

between the IDTs needs only be elastic, as it merely acts as the transmission medium for the SAW [1]. At the receiver IDT, a piezoelectric substrate is required to convert the mechanical wave back into an electrical signal.

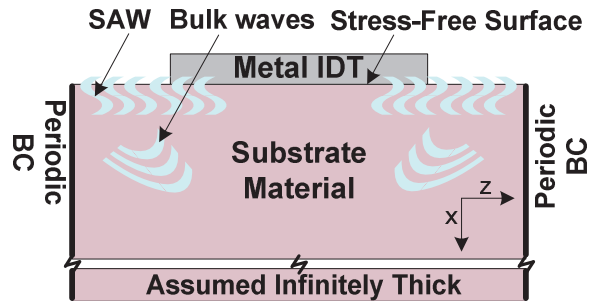


Fig. 2. One IDT finger on the sagittal plane of a SAW device.

Figure 2 shows the sagittal plane (side view) of the SAW device, indicated by the cut line in Fig. 1. SAW waves are generally confined to within one or two wavelengths from the free surface of the substrate material. However, other types of excitations, such as bulk acoustic waves (BAWs) will radiate into the substrate.

In practice, the SAW generation is often also accompanied by some small creation of BAWs, which act as parasitic waves. It is thus required to remove the reflection of these waves from the bottom of the device.

Figure 1 also shows the symmetry of the device with respect to the sagittal cut line. This, along with the assumption that the device is infinitely thick in the y direction, allows for a complete analysis of the device by only studying the sagittal plane. The problem can therefore be analyzed in the xz plane denoting the sagittal plane, thus significantly reducing the computational requirements.

B. Absorbing boundary conditions and the perfectly matched layer

Several absorbing boundary conditions (ABCs) have been suggested with progressive improvements. Most of these ABCs were originally developed for electromagnetic wave propagation [11, 12]. In his 1994 paper, Bérenger described his PML, which offered significant improvement over previous ABCs [10].

In a pioneering work in 1996, Chew and Liu developed a PML for elastodynamics [13]. In 2006, Chagla and Smith introduced a PML for piezoelectric materials by splitting the velocity components into the normal and tangential subcomponents, and only attenuating the normal velocity subcomponents. The resulting absorbing boundary condition showed instabilities for some crystal classes [9]. Here, we introduce losses, not just for the velocity components, but for the stress field subcomponents as well, thereby generalizing the loss matrix. At the same time, by preserving the matching condition throughout, the code remains stable.

C. The PML for electromagnetic wave propagation

The ABC equations for the electromagnetic waves are

$$\varepsilon_0 \frac{\partial \mathbf{E}}{\partial t} + \sigma \mathbf{E} = \nabla \times \mathbf{H}, \quad (1)$$

$$\mu_0 \frac{\partial \mathbf{H}}{\partial t} + \sigma^* \mathbf{H} = -\nabla \times \mathbf{E}, \quad (2)$$

where σ is the conductivity and σ^* is a non-physical quantity that symmetrises the absorption of the magnetic field with that of the electric field [10]. ε_0 , and μ_0 are the permittivity and permeability of the free space, respectively. In order to demonstrate the method, we show the case where a medium is matched to the vacuum. In general however, the computational domain can be matched to any number of media, for instance, a dielectric, an isotropic material, a non isotropic material, or in fact to another PML.

The matching condition in Bérenger's derivation is defined as [14]

$$\frac{\sigma}{\varepsilon_0} = \frac{\sigma^*}{\mu_0}. \quad (3)$$

This impedance matching equation ensures that the impedance of the wave travelling inside the domain matches that of the lossy ABC medium defined by equation (1) and (2). The result is a reflectionless propagation of a normally incident plane wave as it passes through the interface. This

works well at normal incidences. However, the reflection becomes large at grazing angles.

Bérenger addressed this problem, by splitting the field quantities into normal and tangential components and modifying equations (1) and (2). The reflection coefficient with $n=1$ for vacuum, matched to this newly defined lossy medium is given by

$$r = \left(\frac{1 - \cos \theta}{1 + \cos \theta} \right)^n. \quad (4)$$

This reflection coefficient is thus zero for both normal and grazing incidence [14].

III. OUR APPROACH

Here, the PML for the elastodynamic wave propagation on piezoelectric solids is derived in exact parallelism with Bérenger's formulation of the PML for electromagnetic waves [10].

The equations describing the propagation of elastodynamic waves in piezoelectric crystals are [15]

$$\hat{\mathbf{s}}^E \frac{\partial \mathbf{T}}{\partial t} = \nabla_s \mathbf{v}, \quad (5)$$

$$\rho \frac{\partial \mathbf{v}}{\partial t} = \nabla \mathbf{T}. \quad (6)$$

Below is a list of symbols used in the equations along with their definitions:

\mathbf{T}	stress field in abbreviated subscript form (6×1 matrix),
\mathbf{d}	piezoelectric strain coefficient (3×6 matrix),
\mathbf{c}^E	stiffness matrix under constant electric field (6×6 matrix),
\mathbf{s}^E	compliance coefficients matrix under constant electric field (6×6 matrix),
\mathbf{d}'	Transpose of \mathbf{d} ,
\mathbf{v}	particle velocity (3×1 matrix),
ρ	material density,
$\nabla \times$	$\begin{bmatrix} 0 & -\partial/\partial z & \partial/\partial y \\ \partial/\partial z & 0 & -\partial/\partial x \\ -\partial/\partial y & \partial/\partial x & 0 \end{bmatrix}$, and

$$\nabla \cdot = (\nabla_s)' \begin{bmatrix} \partial/\partial x & 0 & 0 & 0 & \partial/\partial z & \partial/\partial y \\ 0 & \partial/\partial y & 0 & \partial/\partial z & 0 & \partial/\partial x \\ 0 & 0 & \partial/\partial z & \partial/\partial y & \partial/\partial x & 0 \end{bmatrix}$$

Here, prime denotes a transpose matrix and c^E is the inverse of s^E . Also,

$$\hat{s}^E = (\hat{c}^E)^{-1} = s^E - d'(\epsilon^T)^{-1}d, \quad (7)$$

is called the stiffening equation which includes the effects of piezoelectricity at zero displacement [15]. In component-form, the first line of equation (5), for a trigonal 3m symmetry class crystal, such as lithium niobate (LiNbO₃) is [15]

$$s_{11} \frac{\partial}{\partial t} T_1 + s_{12} \frac{\partial}{\partial t} T_2 + s_{13} \frac{\partial}{\partial t} T_3 + s_{14} \frac{\partial}{\partial t} T_4 = \frac{\partial v_1}{\partial x}. \quad (8)$$

The PML is defined by introducing losses for the component field variables. The loss terms are introduced in accordance with the existing terms in equation (8).

The form of the stiffness matrix determines which components of the stress field are present, and in turn, which loss terms appear in the PML equation. Accordingly, the number of terms in this equation depends on the choice of substrate material. Similar to electromagnetics, equation (8) is used to develop a Bérenger-like boundary condition.

Equation (8) is split into the normal and tangential field subcomponents in the xz plane, (i.e. no y -dependence) to have

$$\begin{aligned} & s_{11} \frac{\partial}{\partial t} T_{1x} + s_{12} \frac{\partial}{\partial t} T_{2x} + s_{13} \frac{\partial}{\partial t} T_{3x} + s_{14} \frac{\partial}{\partial t} T_{4x} \\ & \psi_{T1} T_{1x} + \psi_{T2} T_{2x} + \psi_{T3} T_{3x} + \psi_{T4} T_{4x} \\ & = \frac{\partial(v_{1x} + v_{1z})}{\partial x} \end{aligned} \quad (9)$$

$$s_{11} \frac{\partial}{\partial t} T_{1z} + s_{12} \frac{\partial}{\partial t} T_{2z} + s_{13} \frac{\partial}{\partial t} T_{3z} + s_{14} \frac{\partial}{\partial t} T_{4z} = 0. \quad (10)$$

where Ψ_{Ti} denote the loss term for the corresponding stress component.

For the computational grid depicted in Fig. 3, where the direction of attenuation is along the x -

axis, the PML equations, in vector form are given by

$$\hat{s}^E \frac{\partial \mathbf{T}_x}{\partial t} + \Psi_T \mathbf{T}_x = \nabla_{sx} \mathbf{v} \quad (11)$$

$$\hat{s}^E \frac{\partial \mathbf{T}_z}{\partial t} = \nabla_{sz} \mathbf{v} \quad (12)$$

$$\rho \frac{\partial \mathbf{v}_x}{\partial t} + \psi_v \mathbf{v}_x = \nabla_x \mathbf{T} \quad (13)$$

$$\rho \frac{\partial \mathbf{v}_z}{\partial t} = \nabla_z \mathbf{T}, \quad (14)$$

where Ψ_T is a 6×6 stress loss tensor containing non zero Ψ_{Ti} components only where the \hat{s}^E matrix has nonzero entries. ψ_v is a non-physical scalar denoting the velocity loss-coefficient, and ∇_{sx} , similar to the ∇_s , is a matrix whose only non-zero entries are $\partial/\partial x$. ∇_{sz} , ∇_x , and ∇_z is similarly defined.

Noting that some coefficients are now tensor quantities, we define the acoustic matching condition as

$$\Psi_T = \frac{\psi_v}{\rho} \hat{s}^E. \quad (15)$$

This relation states that the ratios between the stress and velocity loss-coefficients are the same as the ratios of the field variable coefficients. Similar to the electromagnetic case, the matching condition (15) ensures that the loss-coefficients always maintain the same ratio, even as they progressively increase through the PML.

C. The PML time update equations

The derivation of the PML time update equation for the velocity field is less burdensome. This has been previously reported as [9]

$$\mathbf{v}_x^{n+1/2} = \left(\frac{2 - \Delta t \psi_{v,i}}{2 + \Delta t \psi_{v,i}} \right) \mathbf{v}_x^{n-1/2} + \frac{\Delta t}{\rho} \left(\frac{1}{2 + \Delta t \psi_{v,i}} \right) \nabla_x \mathbf{T}. \quad (16)$$

As for the PML time update equations for the stress field, we start with the first row of equation (11). The same analysis applies to the remaining five rows. The first row of this equation in component form is:

$$\begin{aligned} & s_{11} \frac{\partial}{\partial t} T_{1x} + s_{12} \frac{\partial}{\partial t} T_{2x} + s_{13} \frac{\partial}{\partial t} T_{3x} + s_{14} \frac{\partial}{\partial t} T_{4x} + \\ & + \psi_{T1} T_{1x} + \psi_{T2} T_{2x} + \psi_{T3} T_{3x} + \psi_{T4} T_{4x} \quad (17) \\ & = \frac{\partial(v_{1x} + v_{1z})}{\partial x}. \end{aligned}$$

Applying the time-averaging, for quantities at time n and using a central difference scheme for approximating the time derivatives, equation (17) becomes

$$\begin{aligned} & s_{11} \left(\frac{T_{1x} \Big|_{i,j}^{n+1/2} - T_{1x} \Big|_{i,j}^{n-1/2}}{\Delta t} \right) + s_{12} \left(\frac{T_{2x} \Big|_{i,j}^{n+1/2} - T_{2x} \Big|_{i,j}^{n-1/2}}{\Delta t} \right) + \\ & + s_{13} \left(\frac{T_{3x} \Big|_{i,j}^{n+1/2} - T_{3x} \Big|_{i,j}^{n-1/2}}{\Delta t} \right) + s_{14} \left(\frac{T_{4x} \Big|_{i,j}^{n+1/2} - T_{4x} \Big|_{i,j}^{n-1/2}}{\Delta t} \right) + \\ & + \psi_{T1} \left(\frac{T_{1x} \Big|_{i,j}^{n+1/2} + T_{1x} \Big|_{i,j}^{n-1/2}}{2} \right) + \psi_{T2} \left(\frac{T_{2x} \Big|_{i,j}^{n+1/2} + T_{2x} \Big|_{i,j}^{n-1/2}}{2} \right) + \\ & + \psi_{T3} \left(\frac{T_{3x} \Big|_{i,j}^{n+1/2} + T_{3x} \Big|_{i,j}^{n-1/2}}{2} \right) + \psi_{T4} \left(\frac{T_{4x} \Big|_{i,j}^{n+1/2} + T_{4x} \Big|_{i,j}^{n-1/2}}{2} \right) \quad (18) \\ & = \frac{\partial(v_{1x} + v_{1z})}{\partial x}. \end{aligned}$$

Grouping the terms at time $n+0.5$ yields the time update equation

$$\begin{aligned} & (2s_{11} + \Delta t \psi_{T1}) T_{1x} \Big|_{i,j}^{n+1/2} + (2s_{12} + \Delta t \psi_{T2}) T_{2x} \Big|_{i,j}^{n+1/2} + \\ & + (2s_{13} + \Delta t \psi_{T3}) T_{3x} \Big|_{i,j}^{n+1/2} + (2s_{14} + \Delta t \psi_{T4}) T_{4x} \Big|_{i,j}^{n+1/2} + \\ & = (2s_{11} - \Delta t \psi_{T1}) T_{1x} \Big|_{i,j}^{n-1/2} + (2s_{12} - \Delta t \psi_{T2}) T_{2x} \Big|_{i,j}^{n-1/2} + \\ & + (2s_{13} - \Delta t \psi_{T3}) T_{3x} \Big|_{i,j}^{n-1/2} + (2s_{14} - \Delta t \psi_{T4}) T_{4x} \Big|_{i,j}^{n-1/2} + \\ & 2\Delta t \frac{\partial(v_{1x} + v_{1z})}{\partial x}. \quad (19) \end{aligned}$$

For all rows, the result can be cast in the more concise matrix form

$$(2\hat{s}^E + \Delta t \Psi_T) \mathbf{T}_x \Big|_{i,j}^{n+1/2} = (2\hat{s}^E - \Delta t \Psi_T) \mathbf{T}_x \Big|_{i,j}^{n-1/2} + 2\Delta t \nabla_x \mathbf{v}. \quad (20)$$

Making use of the matching condition defined in equation (15) to substitute for Ψ_T , we have:

$$\begin{aligned} & (2\hat{s}^E + \Delta t \hat{s}^E \frac{\psi_v}{\rho}) \mathbf{T}_x \Big|_{i,j}^{n+1/2} = \quad (21) \\ & (2\hat{s}^E - \Delta t \hat{s}^E \frac{\psi_v}{\rho}) \mathbf{T}_x \Big|_{i,j}^{n-1/2} + 2\Delta t \nabla_x \mathbf{v}. \end{aligned}$$

Multiplying by $\hat{\mathbf{c}}^E$ which is the inverse of $\hat{\mathbf{s}}^E$ the time update equation within the PML becomes

$$\mathbf{T}_x^{n+1/2} = \frac{\xi_v}{\xi_v^*} \mathbf{T}_x^{n-1/2} + \frac{2\Delta t}{\xi_v^*} \hat{\mathbf{c}}^E \nabla_x \mathbf{v} \quad (22)$$

where $\xi_v = (2 - \Delta t \psi_v / \rho)$ and $\xi_v^* = (2 + \Delta t \psi_v / \rho)$. It should be noted that the quantities ξ_v and ξ_v^* are scalars. There is no need for matrix inversion. This significantly relaxes the computational resources for calculating the field values inside the PML. The T_z component of the stress field is allowed to propagate without loss, and the equation is given by

$$T_z^{n+1/2} = T_z^{n-1/2} + \Delta t \hat{\mathbf{c}}^E \nabla_z \mathbf{v}. \quad (23)$$

The end of the boundary is often terminated with a perfect reflector. This ensures that any reflections from the terminal layer of the PML undergo a secondary attenuation upon return.

The matching condition is in essence a constraint, which connects the loss-coefficients of the stress and velocity fields. That is, setting ψ_v is sufficient for defining both equations (16) and (22). Note that these two equations define one layer of the PML. An arbitrary number of layers can be specified. Generally the more layers the PML has, the better it is in suppressing reflections.

From one layer to the next, starting at the medium-PML interface, the loss-coefficients are gradually increased according to a profile function. At the starting layer, the loss-profile ψ_v is small; however, it is ramped up at every layer, terminating at a final value $\psi_{v,0}$ at the end of the PML. Generally, either a polynomial or exponential loss profile is employed to define the sequence of ψ_v values, as is done in electromagnetics. We have used a polynomial loss profile given by [14]

$$\psi_{v,i} = \psi_{v,0} \left(\frac{i - x_{PML}}{\delta} \right)^m, \quad (24)$$

where x_{PML} is the position of the onset of the PML, i is the position of each PML, δ is the thickness of the PML, $\psi_{v,0}$ is the loss-coefficient at the terminal layer of the PML, and m is the order of the polynomial used. $\psi_{v,0}$ is either chosen heuristically, or using an empirical formula similar to the electromagnetic PML explained in [12].

IV. RESULTS AND DISCUSSION

Figure 3 shows the computational domain, which is the discretized sagittal plane depicted in Fig. 2. The domain is terminated on the left and the right sides by periodic boundaries, modelling an infinite interdigital transducer (IDT). This is the case, for example, in a SAW resonator, where the excitation travels symmetrically in both directions.

A. Point-excitation in the vicinity of the PML

The first example addresses the case of a point excitation in the vicinity of the PML. The domain is one IDT period of the sagittal plane shown in Fig. 2 with the assumption that the IDT is infinitely long compared to the wavelength of the SAW. This reduces the problem to a two dimensional analysis in the sagittal plane. A spatial resolution of 33.57×10^{-5} m, and a temporal timestep of 0.318 ns are used on a 91×91 grid.

The PML was tested for sinusoidal, Gaussian, and impulse excitations placed 8 spatial steps from a PML with 15 layers. The relative amplitude of reflection for all excitations, was less than 10^{-6} after 6000 timesteps or 19 μ s.

The implemented PML is used for the bottom of the domain. This allows any unwanted parasitic waves to be removed from the computational domain, as though the computational domain were a semi-infinite plane. Any other boundary condition will result in spurious reflections from the bottom that will show up in the detection IDT of the device as computational noise.

The top boundary condition is stress-free, implying that all components of the stress normal to the boundary (i.e. T_1 , T_5 , T_6) are set to zero [8]. Therefore, at the stress-free boundary, the only non-zero components of the stress are the transverse ones.

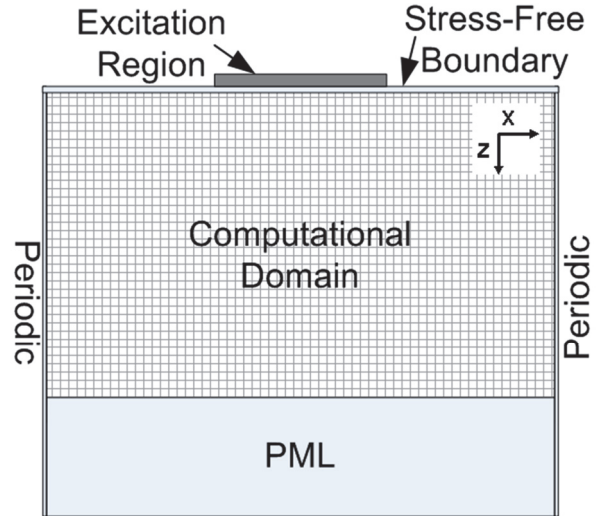


Fig. 3. The computational domain.

A Gaussian-modulated sinusoidal with a center frequency of 1.0 GHz is applied to the middle of the free surface. This excitation is applied to the T_3 component of the wave which is a compressional stress component in the z -direction.

Figure 4 shows the plot of the v_l component of the field in an unbounded region, where the wave is freely propagating (solid curve) vs. the same measurement when one side of the boundary is terminated by a PML. The two curves are virtually overlapping and the reflection is under 10^{-6} as seen in Fig. 4.

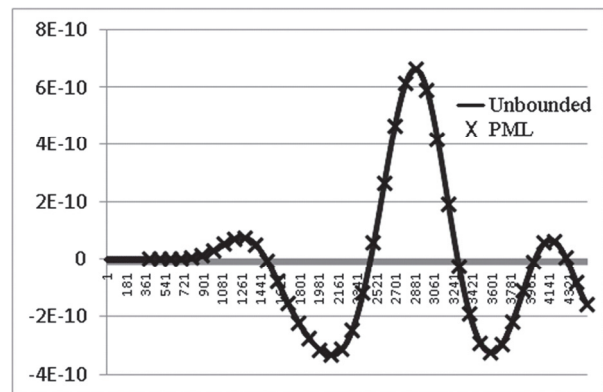
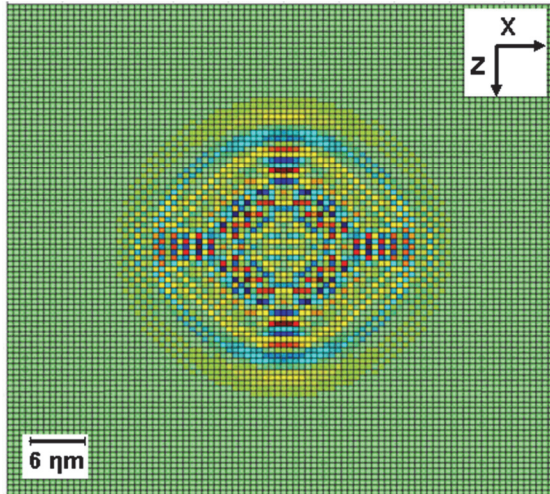
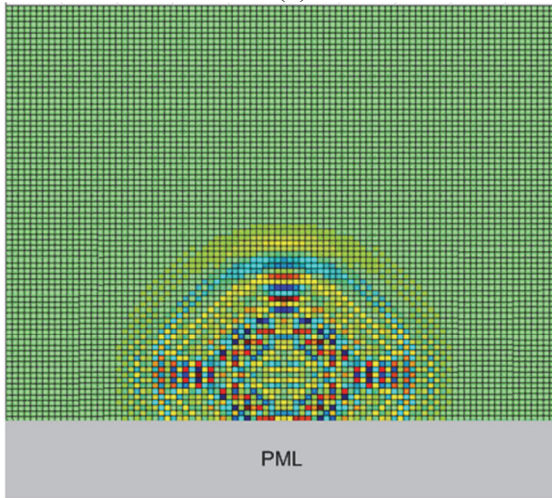


Fig. 4. A comparison of reflection of the normalized v_l field component for an unbounded medium and a PML-bounded medium. The vertical axes is the amount of reflection from the boundary and the horizontal axes denotes the number of timesteps.



(a)



(b)

Fig. 5. v_l field component of an excitation near the PML; (a) A sinusoidal excitation in an unbounded region, and (b) symmetric spread of the same excitation near the PML after $15.9 \mu\text{s}$ or 5000 time steps.

Figure 5(a) shows the propagation of the wave in the unbounded region while Fig. 5(b), shows the field near the boundary after $15.9 \mu\text{s}$. The two profiles are identical for the domain region outside the PML. The symmetric shape of the excitation is preserved even after a prolonged interaction with the PML.

B. Line-excitation via a metallic IDT

Figure 6 shows the excitation under the metallic IDT in the computational domain of Fig. 2. The excitation for this example is a line source underneath the metallic strip. A Gaussian-

modulated time profile with a center frequency of 1.0 GHz is also used in this example. The crystal cut is chosen as 128 X-Cut Y propagating lithium niobate. The main excitation type is of Rayleigh type; with some bulk waves also excited.

If these excitations are not removed, they introduce computational noise, shown in Fig 7(a) where the domain is not terminated with a PML. The reflections are magnified in the figure near their corresponding boundaries.

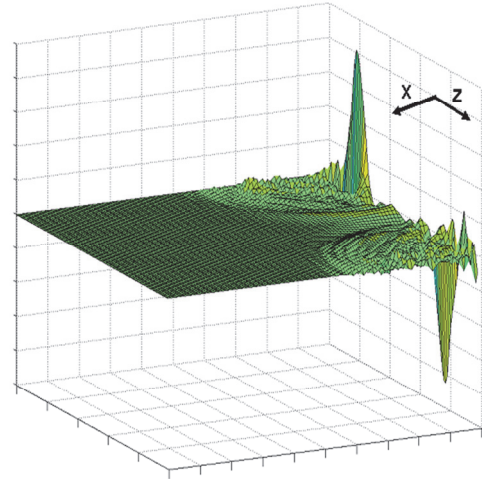


Fig. 6. v_l field component of a line excitation of a SAW on the surface of the piezoelectric material.

However, by introducing a PML-terminated computational domain in Fig. 7(b), these spurious reflections are effectively removed, and are not reintroduced into the computational domain.

V. CONCLUSION

A matching condition is developed for the implementation of a perfectly matched layer for propagation of waves in piezoelectric materials. The new matching condition preserves the impedance matching criteria for all components of the stress and velocity fields. Coupled piezoelectric waves require a more elaborate matching condition to preserve the wave impedance in the PML region. We plan on further reducing the reflections by choosing PML grading optimized for all wave components.

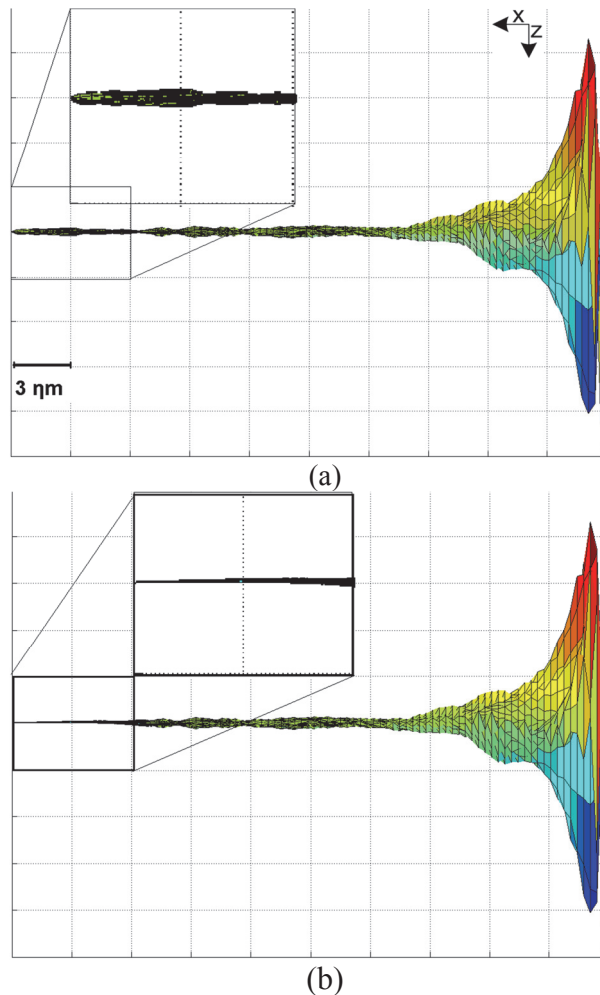


Fig. 7. Snapshots of the v_l component of the acoustic waves inside the device (a) SAW and BAW generated in a medium without PML on the left boundary. (b) Same IDT excitation terminated with PML.

REFERENCES

- [1] C. K. Campbell, *Surface Acoustic Wave Devices for Mobile and Wireless Communications*, Academic Press, New York, 1998.
- [2] P. Ventura, J. M. Hode, M. Solal, J. Desbois, and J. Ribbe, "Numerical Methods for SAW Propagation Characterization," *IEEE Ultrasonics Symposium*, vol. 1, pp. 176-186, 1998.
- [3] K. Y. Hashimoto, *Surface Acoustic Wave Devices in Telecommunications. Modelling and Simulation*, Springer, 2000.
- [4] P. Ventura, J. M. Hode, and M. Solal, "A New Efficient Combined FEM and Periodic Green's Function Formalism for the Analysis of Periodic SAW Structures," *IEEE Ultrasonics Symposium*, vol. 1, pp. 263-268, 1995.
- [5] K. Y. Hashimoto, "Simulation of Surface Acoustic Wave Devices," *Jap. J. of App. Phys.*, vol. 45, no. 5B, pp. 4423-4428, 2006.
- [6] K. Y. Hashimoto, T. Omori, and M. Yamaguchi, "Analysis of SAW Excitation and Propagation under Periodic Metallic Grating Structures," *International J. of High Speed Electronics and Systems*, Singapore, World Scientific Publishing, vol. 10, no. 3, pp. 685-734, 2000.
- [7] C. C. W. Ruppel, W. Ruile, G. Scholl, K. C. Wagner, and O. Manner, "Review of Models for Low-Loss Filter Design and Applications," *IEEE Ultrasonics Symposium*, vol. 1, pp. 313-324, 1994.
- [8] K. Y. Wong and W. Y. Tam, "Analysis of the Frequency Response of SAW Filters using Finite-Difference Time-Domain Method," *IEEE Trans. on Microwave Theory and Techniques*, vol. 53, no. 11, 2005.
- [9] F. Chagla and P. Smith, "Finite Difference Time Domain Methods for Piezoelectric Crystals," *IEEE Trans. on Ultras. Ferroelec. and Freq. Cont.*, vol. 53, no. 10, 2006.
- [10] J. P. Bérenger, "A Perfectly Matched Layer for the Absorption of Electromagnetic Waves," *J. of Computational Physics*, vol. 114, issue 2, pp. 185-200, 1994.
- [11] R. Mittra and M. Kuzuoglu, "A Review of Some Recent Advances in Perfectly-Matched Absorbers for Mesh Truncation in FEM," *IEEE Antennas and Propagation Society International Symposium*, vol. 2, pp. 1302-1305, 1997.
- [12] A. Taflove and S. C. Hagness, *Computational Electrodynamics: The Finite-Difference Time-Domain Method*, 2nd ed. Norwood, MA, Artech House, 2000.
- [13] W. C. Chew and Q. H. Liu, "Perfectly Matched Layers for Elastodynamics: A New Absorbing Boundary Condition," *J. of Comp. Acoust.*, vol. 4, no. 4, pp. 341-360, 1996.
- [14] J. P. Bérenger, *Perfectly Matched Layer (PML) for Computational Electromagnetics*, 1st ed., Morgan & Claypool, 2007.

- [15] B. A. Auld, *Acoustic Fields and Waves in Solids*, 2nd ed., New York, Kruger Publishing Co., 1990.



Arthur Montazeri received his B.Eng. in Engineering Physics at McMaster University in 2004. He then joined the Department of Physics and Astronomy at McMaster University, as a Research Assistant studying the diffusion of macro-molecules in the dense cellular environment. He earned his M.A.Sc. degree in Electrical and Computer Engineering from McMaster University in 2010, and is currently a Ph.D. student at the ECE Department at McMaster University. His research interests include modeling physical media and wave propagation using numerical techniques, and studying novel approaches for high efficiency solar conversion systems.



Mohamed Bakr received a B.Sc. and M.Sc. degrees in Electronics and Communications Engineering and Engineering Mathematics from Cairo University, Egypt in 1992 and 1996, respectively with distinction (honors). From 1998 to 2000, he worked as a research assistant with the Simulation Optimization Systems (SOS) research laboratory, McMaster University, Hamilton, Ontario, Canada. He earned the Ph.D. degree in September 2000 from the Department of Electrical and Computer Engineering, McMaster University. In November 2000, he joined the Computational Electromagnetics Research Laboratory (CERL), University of Victoria, Victoria, Canada as an NSERC Post Doctoral Fellow. His research areas of interest include computer-aided design and modeling of microwave and photonic circuits, neural network applications, efficient optimization using time/frequency domain methods, and bioelectromagnetism. He is a main contributor to the theories of electromagnetic adjoint sensitivities and space mapping optimization. He is currently an associate professor with the Department of

Electrical and Computer Engineering, McMaster University.



Yaser M. Haddara received a B.Eng. in Electrical Engineering from Memorial University of Newfoundland, St. John's, Newfoundland, in 1991, and an M.S. and Ph.D. from Stanford University, CA, in 1993 and 1997. He was a postdoctoral research associate at the University of Florida, Gainesville, FL, and was a Senior Engineer in the device group at Cypress Semiconductor. He is currently an Associate Professor in Electrical & Computer Engineering at McMaster University, Hamilton, Ontario and has been at McMaster since 2002. Dr. Haddara's research interests are in front-end silicon and silicon-germanium process modeling, nanowires growth and modeling technology CAD, and RF circuit design. His teaching interests are in microelectronics, device physics, process modeling, and probability and statistics.